THE ASTROPHYSICAL JOURNAL, 362:354–363, 1990 October 10

TITAN'S UPPER IONOSPHERE

W.-H. IP
Max-Planck-Institut für Aeronomie
Received 1989 July 18; accepted 1990 April 10

ABSTRACT

As a result of electron impact ionization and photoionization, an ionosphere should be built up at the high-altitude region of Titan's atmosphere. From a simple consideration of the Chapman layer theory, the peak electron density can be determined to be $\approx 5 \times 10^3$ cm^{-3} at about 1200 km altitude. The complex ion-molecule reactions in the N_2–CH_4 atmosphere would lead to a mixture of N_2^+, CH_3^+, $C_2H_5^+$, and H_2CN^+ ions as the major ion species in the upper ionosphere. The new calculations presented here also predict the presence of significant amounts of CH_5^+, N_2H^+, $C_2H_2^+$, and $C_2H_3^+$ ions (i.e., $n_i \approx 10$–100 cm^{-3}) near the ionospheric peak. Because of fast ion-neutral reactions with CH_4 and N_2, the number density of the Ar^+ ions would not exceed a value of more than 10 cm^{-3} in the upper ionosphere if argon has a mixing ratio about 10^{-2} near the homopause. Interaction with the partially corotating magnetospheric plasma could lead to a significant modification of the ionospheric profile in the high altitudes. The ionospheric flow dynamics are studied in the limits of one-fluid mass-loaded flow and of diffusion-convection approximation. Both approaches show that ion-neutral friction acts as a cushion against plasma streaming effects.

Subject headings: molecular processes — planets: abundances — planets: magnetospheres — planets: satellites — planets: Saturn

I. INTRODUCTION

The *Voyager 1* encounter with Titan in 1980 has shown that Titan's thick atmosphere with a surface pressure of 1.5 bars is mainly composed of nitrogen and methane (Broadfoot *et al.* 1981, Hanel *et al.* 1981; Tyler *et al.* 1981; Hunten *et al.* 1984). The relatively large scale height of the neutral atmosphere permits a very extended structure of the exosphere. The exobase has been estimated to be located at about 1400 km altitude (Smith *et al.* 1982). In comparison, exobases of the terrestrial planets with no or very weak intrinsic magnetic fields (i.e., Venus and Mars) are all below 200 km altitude. This unique feature therefore places the Titan interaction with the solar wind or the magnetospheric plasma in a different category from those of Venus and Mars (Russell and Vaisberg 1983). This point can be demonstrated by scaling the magnetosphere of Venus to Titan in the case of solar wind interaction (see Fig. 1). At the subsolar point, the scaled bow shock and ionopause positions would be located below Titan's exobase. Obviously, in this region ion-neutral frictional interaction must play an important role in shaping Titan's plasma interaction as well as its ionospheric structure.

Another interesting feature is that in the magnetospheric environment of Saturn, suprathermal electrons are the major ionizing agent, while the solar EUV radiation is much less effective (Sittler, Ogilvie, and Scudder 1983; Strobel and Shemansky 1982; Hartle *et al.* 1982; Hunten *et al.* 1984). The spectral signatures of the Rydberg bands of N_2 (N_2RYD), the N I multiplet at 1134 Å, and the N II multiplet at 1085 Å indicated that the bombarding electrons should have an energy of about 20 eV (Broadfoot *et al.* 1981; Strobel and Shemansky 1982). During the *Voyager* observations, Titan was inside Saturn's magnetosphere, and it is quite probable that precipitation of magnetospheric electrons could be responsible for the impact excitation of the N_2 emission (Hartle *et al.* 1982; Hartle 1984). The atmospheric absorption effect of the magnetospheric electrons is consistent with the *Voyager* plasma observations that in the wake of Titan the electron population with $kT_e > 700$ eV was highly depleted (Bridge *et al.* 1981). For this mechanism to be effective, Hartle *et al.* (1982) invoked the curvature drift effect of the suprathermal electrons in the draped magnetic field geometry around Titan. In other words, as a result of the centrifugal drift with a force $F_c = meV_{\|}^2/R$ on one hemisphere (the sunlit side during the *Voyager* encounter), an electron, with a field-aligned velocity of $V_{\|}$ along a curved magnetic field with a radius of curvature R, will drift toward the lower atmosphere where collisional probability is higher. Because of the slowdown of the motion of the magnetospheric plasma flow in the vicinity of Titan, the drifting electrons would have enough time to pass through the exosphere (column density $> 10^{15}$ cm^{-2}) many times, so that they could be lost via inelastic scattering or ionization loss. The energy decrement due to ionization loss is typically on the order of $\Delta E \approx 35$ eV per electron. For keV electrons with a flux of about 2×10^7 cm^{-2} s^{-1}, the effective ionizing flux is thus $f_e \approx 6 \times 10^8$ cm^{-2} s^{-1}.

It should be mentioned that in the particle precipitation process, the secondary electron population plays an important role in the excitation, dissociation, and ionization of the nitrogen atmosphere. The detailed morphology depends on a number of factors, i.e., the draped magnetic field configuration, the elastic and inelastic scattering of the primary electrons, and the transport of the secondary electrons in Titan's atmosphere. To treat this problem properly, very careful numerical computations would have to be performed to simulate the altitude profiles of the pertinent ionization rate. Such a detailed treatment is outside the scope of this work of exploratory nature. In the present simplified model, we approximate the attenuation of the ionizing electron flux by adopting the Chapman theory of ionospheric formation (Bauer 1973, 1985). That is, the peak of the ionospheric electron density is situated at the altitude (z_0) where the optical depth of the atmosphere for the ionizing

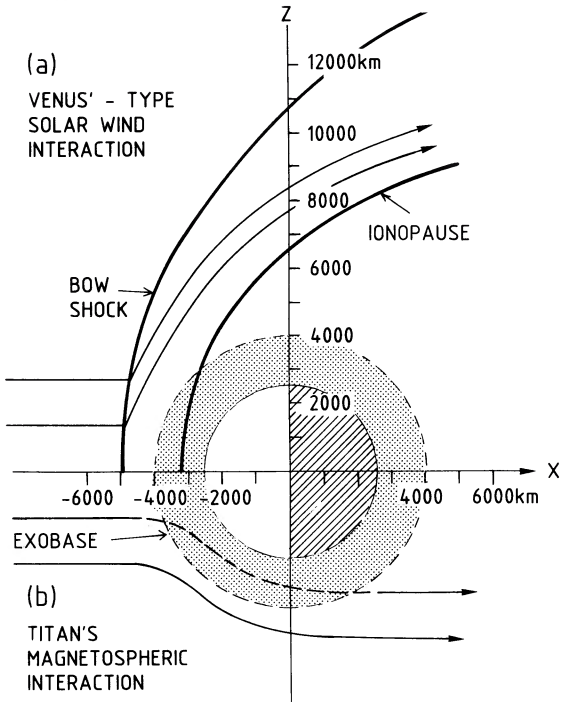

FIG. 1.—Comparison of (*a*) the Venus-type solar wind interaction and (*b*) the magnetospheric interaction of Titan. The shaded region denotes the atmosphere below the exobase.

source reaches unity. With the optical depth defined as

$$\tau = \int_{\infty}^{z} n\sigma_i dz \,, \tag{1}$$

we find $\tau = 1$ at $z_0 = 1240$ km if $\sigma_i = 2 \times 10^{-16}$ cm^2. The atmospheric gas density at z_0 is $n_0 = 1.2 \times 10^9$ cm^{-3}.

In the following calculation, the photoionization effect is also included by assuming an ionization flux of 5×10^7 photons cm^{-2} s^{-1} and an ionization cross section of 2×10^{-17} cm^2. The corresponding Chapman layer is found to be at ≈ 1000 km altitude.

The peak electron density can be approximated by balancing the electron impact ionization rate with the electron dissociative recombination rate. In other words, we have

$$f_e \exp(-\tau)\sigma_i n_0 \approx \langle\alpha\rangle n_e^2 \,, \tag{2}$$

where f_e is the ionizing electron flux at large distances from Titan and $\langle\alpha\rangle$ is the effective electron dissociative recombination coefficient.

In Titan's ionosphere, different ion species have different values of electron dissociative recombination coefficients (α). For example, the α-value of N_2 ions is 2×10^{-7} cm^3 s^{-1}, whereas the corresponding value for $C_2H_5^+$ ions is 2×10^{-6} cm^3 s^{-1}, and it is 6×10^{-7} cm^3 s^{-1} for H_2CN^+ ions. The effective value of α at different altitudes is thus determined by the dominant ions locally. As will be discussed in § III, near the ionospheric peak at 1200 km altitude the most abundant ions are H_2CN^+ and $C_2H_5^+$, with a ratio of approximately 3:1. The effective value of the electron dissociative recombination coefficient is thus 10^{-6} cm^3 s^{-1}. Now with $f_e = 5 \times 10^8$ cm^2 s^{-1} and $\alpha \approx 10^{-6}$ cm^3 s^{-1}, we have $n_e \approx 5000$ cm^{-3}. This value is in agreement with one of the upper limits of 5×10^3 cm^{-3} derived from the *Voyager 1* radio occultation experiment (Lindal *et al.* 1983; Bauer 1985; McNutt and Richardson 1988). In addition to the different rates in electron dissociative recombination loss, the ions also follow different paths in the ion-molecule reactions. A combination of ion-neutral reactions and electron dissociation recombination loss therefore determines the basic nature of the ion composition in Titan's ionosphere. In the present work, a comprehensive set of ion-neutral reactions in the N_2–CH_4 atmosphere is included in the chemical network. This new study indicates important differences in the major ion composition in the upper ionosphere from an earlier work by Bauer (1985).

Finally, from *Voyager* observations it was found that the subsolar point of the magnetopause of the Saturnian magnetosphere is nominally outside the orbit of Titan (see Behannon, Lepping, and Ness 1983). Only during strong compression events of large solar wind dynamical pressure would Titan encounter the solar wind. For this reason, we shall focus on Titan's magnetospheric interaction only. In other words, we shall assume that the corotating plasma flow is sub-Alfvénic and that no shock will form in the interaction process (see Bridge *et al.* 1981; Neubauer *et al.* 1984).

II. BASIC STEPS

a) Chemical Reactions

The mixing ratios of several major molecules in Titan's upper atmosphere computed by Yung, Allen, and Pinto (1984) are shown in Figure 2. Superposed on these one-dimensional photochemical model calculations is the profile of the mixing ratio of CO estimated from ground-based observations (Lutz, de Bergh, and Owen 1983; Muhleman, Berge, and Clancy 1984; Marten *et al.* 1988). Note that in addition to the minor species (C_2H_2, C_2H_4, C_2H_6, C_2N_2, HCN, HC_3N, and C_2N_2) shown, other complex molecules have also been identified from infrared spectra of the *Voyager* IRIS experiments (Hanel *et al.* 1981; Hunten *et al.* 1984). These hydrocarbons are products of photolysis in the upper atmosphere of Titan (Strobel 1974, 1982). Their subsequent precipitation and condensation in the

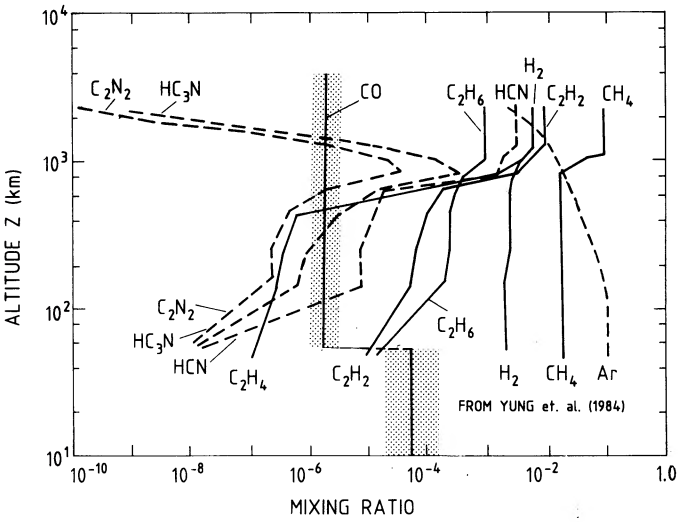

FIG. 2.—Mixing ratios of gas species used in the calculations. The vertical profiles are adopted from the one-dimensional photochemical models by Yung, Allen, and Pinto (1984). The CO profile is adopted from the ground-based radio observation at 115 GHz by Marten *et al.* (1988). Argon is assumed to have a mixing ratio of 0.01 at the homopause.

lower region would provide the source material for the orange-colored aerosol particles.

The neutral and ion species considered in the present work are listed in Table 1. The computer program is capable of including CO, CO_2, H_2O, and Ar (and their corresponding ions) in the chemical network. Argon, in particular, is of interest, as it has been postulated to be a significant gas component with a mixing ratio of up to 15% (Samuelson *et al.* 1981; Owen 1982). It should be noted that arguments have also been presented for the case of a much smaller abundance of argon in Titan's atmosphere (Lindal *et al.* 1983).

The mixing ratio of CO has been discovered to be 6×10^{-5} by Lutz, de Bergh, and Owen (1983) from ground-based near-infrared spectra (≈ 1.6 μm). A similar value of the CO abundance ($7.5^{+10.5}_{-4.5} \times 10^{-5}$) was obtained by Muhleman, Berge, and Clancy (1984) from radio observations of the CO (1–0) line emission at 115 GHz. However, in a later millimeter observation at the same line by Marten *et al.* (1988), a much lower value [$(1–2) \times 10^{-6}$] was obtained. H_2O so far has not been identified. There is, however, good reason to suspect its presence as a result of continuous influx of interplanetary meteoroids (Yung, Allen, and Pinto 1984; Ip 1990). The detected CO molecules, for example, must originate from such meteor-atmosphere interaction. Finally, CO_2 has been determined to have a mixing ratio of 1.5×10^{-9} from the *Voyager* IRIS observations (Samuelson *et al.* 1983).

TABLE 1

SPECIES INVOLVED IN PHOTOCHEMISTRY OF TITAN'S ATMOSPHERE[a]

Neutral Species	Mass[b]	Ion Species	Mass[b]
H	1	H_2^+	2
H_2	2	H_3^+	3
CH_4	16	CH^+	13
C_2H_2	26	CH_2^+	14
C_2H_4	28	CH_3^+	15
C_2H_6	30	CH_4^+	16
N	14	CH_5^+	17
N_2	28	C_2H^+	25
HCN	27	$C_2H_2^+$	26
CH_3CN	51	$C_2H_3^+$	27
C_2N_2	52	$C_2H_5^+$	29
(CO)	28	$C_2H_6^+$	30
(CO_2)	44	C_3H^+	37
(H_2O)	18	N^+	14
(Ar)	36	N_2^+	28
		N_2H^+	29
		(H_2O^+)	18
		(H_3O^+)	19
		(Ar^+)	36
		(ArH^+)	37
		CN^+	26
		HCN^+	27
		H_2CN^+	28
		C_2N^+	38
		C_3N^+	50
		HC_3N^+	51
		$C_2N_2^+$	52
		$HC_2N_2^+$	53
		(CO^+)	28
		(HCO^+)	29
		(CO_2^+)	44
		(HCO_2^+)	45

[a] Species in parentheses not considered in the present work.

[b] Atomic or molecular mass in amu.

The ion-molecule reaction rates are adopted from the handbook compiled by Anicich and Huntress (1986). The full set of the reactions used in this work is listed in Table 2. Complementary to the ion-molecule reactions, we have listed electron impact ionization processes for the major species. They are included in Table 3. Electron dissociative recombination losses for the molecular ions are characterized by

$$AB^+ + e \rightarrow A + B ,$$

with the pertinent recombination coefficients given in Table 4.

In addition to the magnetospheric suprathermal electron impact ionization, the ionization effect of Galactic cosmic-ray (GCR) particles is also of importance. Previous work by Capone *et al.* (1980) has shown that a very substantial ion density in the lower atmosphere of Titan at altitude below a few hundred kilometers could be produced via cosmic-ray–induced ionization. The GCR ionization flux at infinity is given to be $f_{CR} = 6.7 \times 10^5$ cm^{-2} s^{-1}. The pertinent absorption cross section is $\sigma_{CR} = 5.0 \times 10^{-23}$ cm^2. The ionization rate at altitude z is therefore

$$\dot{n}_{CR} = f_{CR}\, \sigma_{CR} \exp(-\tau_{CR}) , \quad (3)$$

where

$$\tau_{CR} = \int_{\infty}^{z} n \sigma_{CR}\, dz .$$

Now, assuming a one-dimensional geometry, appropriate to a plasma flow streaming along the central axis in the corotation direction, the continuity equation of certain ion species i can be expressed as

$$\frac{\partial n_i}{\partial t} + \frac{\partial}{\partial z}(n_i w_i) = q_i - l_i , \quad (4)$$

where n_i is the number density, w_i the vertical flow velocity, q_i the production rate from electron impact ionization and ion-molecule reactions, and l_i the loss rate due to ion-molecule reactions and electron dissociative recombination. In the computations, we assume a steady state condition, thus $\partial n_i/\partial t = 0$, and that all ion species move at the same speed.

It is important to note that all important chemical reactions must be taken into account in the ionospheric chemical network if the correct ion composition is to be modeled. As will be discussed further below, the inclusion of all major reactions would produce an ionosphere with N_2^+ and N^+ as the major ions in the upper region, with CH_3^+ as the second or third most important ion species for altitudes above 1500 km. On the other hand, the omission of the reactions of CH_3^+ with neutral species such as

$$CH_3^+ + CH_4 \rightarrow C_2H_5^+ + H_2 \quad (5)$$

would lead to a CH_3^+–rich ionosphere as described earlier by Bauer (1985).

Because vertical profiles of neutral abundance in the model calculations by Yung, Allen, and Pinto (1984) extend only up to 1200 km altitude, the mixing ratios beyond must be extrapolated. The most important species is naturally CH_4. We have

TABLE 2

LIST OF ION-MOLECULE REACTIONS IN TITAN'S ATMOSPHERE

	Process	Branching Ratio	Rate Coefficient
(1)	$H_2^+ + H_2 \rightarrow H_3^+ + H$	1.00	0.640E−09
(2)	$H_2^+ + CH_4 \rightarrow CH_5^+ + H$	0.03	0.380E−08
(3)	$H_2^+ + CH_4 \rightarrow CH_4^+ + H_2$	0.37	0.380E−08
(4)	$H_2^+ + CH_4 \rightarrow CH_3^+ + H_2$	0.60	0.380E−08
(5)	$H_2^+ + C_2H_2 \rightarrow C_2H_3^+ + H$	0.09	0.530E−08
(6)	$H_2^+ + C_2H_2 \rightarrow C_2H_2^+ + H_2$	0.91	0.530E−08
(7)	$H_2^+ + C_2H_4 \rightarrow C_2H_3^+ + H_2$	0.37	0.490E−08
(8)	$H_2^+ + C_2H_4 \rightarrow C_2H_2^+ + H_2$	0.18	0.490E−08
(9)	$H_2^+ + C_2H_6 \rightarrow C_2H_6^+ + H_2$	0.06	0.490E−08
(10)	$H_2^+ + C_2H_6 \rightarrow C_2H_5^+ + H_2$	0.28	0.490E−08
(11)	$H_2^+ + C_2H_6 \rightarrow C_2H_3^+ + H_2$	0.14	0.490E−08
(12)	$H_2^+ + C_2H_6 \rightarrow C_2H_2^+ + H_2$	0.04	0.490E−08
(13)	$H_2^+ + N_2 \rightarrow N_2H^+ + H$	1.00	0.200E−08
(14)	$H_2^+ + Ar \rightarrow ArH^+ + H$	1.00	0.124E−08
(15)	$H_3^+ + CH_4 \rightarrow CH_5^+ + H_2$	1.00	0.240E−08
(16)	$H_3^+ + C_2H_2 \rightarrow C_2H_3^+ + H_2$	1.00	0.290E−08
(17)	$H_3^+ + C_2H_4 \rightarrow C_2H_5^+ + H_2$	0.30	0.230E−08
(18)	$H_3^+ + C_2H_4 \rightarrow C_2H_3^+ + H_2$	0.70	0.230E−08
(19)	$H_3^+ + C_2H_6 \rightarrow C_2H_5^+ + H_2$	1.00	0.240E−08
(20)	$H_3^+ + N_2 \rightarrow N_2H^+ + H_2$	1.00	0.180E−08
(21)	$H_3^+ + Ar \rightarrow ArH^+ + H_2$	1.00	0.100E−09
(22)	$H_3^+ + HCN \rightarrow H_2CN^+ + H_2$	1.00	0.950E−08
(23)	$H_3^+ + C_2N_2 \rightarrow HC_2N_2^+ + H_2$	1.00	0.220E−08
(24)	$CH^+ + H_2 \rightarrow CH_2^+ + H$	1.00	0.140E−08
(25)	$CH^+ + CH_4 \rightarrow C_2H_3^+ + H_2$	0.84	0.130E−08
(26)	$CH^+ + CH_4 \rightarrow C_2H_2^+ + H_2$	0.11	0.130E−08
(27)	$CH^+ + N \rightarrow CN^+ + H$	1.00	0.190E−09
(28)	$CH^+ + HCN \rightarrow H_2CN^+ + C$	0.75	0.240E−08
(29)	$CH^+ + HCN \rightarrow C_2N^+ + H_2$	0.15	0.240E−08
(30)	$CH^+ + HCN \rightarrow H_2CN^+ + C$	1.00	0.280E−08
(31)	$CH_2^+ + H_2 \rightarrow CH_3^+ + H$	1.00	0.720E−09
(32)	$CH_2^+ + CH_4 \rightarrow C_2H_5^+ + H$	0.30	0.120E−08
(33)	$CH_2^+ + N \rightarrow CN^+ + H_2$	1.00	0.220E−09
(34)	$CH_3^+ + H_2 \rightarrow CH_5^+$	1.00	0.110E−12
(35)	$CH_3^+ + CH_4 \rightarrow C_2H_5^+ + H_2$	1.00	0.120E−08
(36)	$CH_3^+ + C_2H_4 \rightarrow C_2H_3^+ + CH_4$	0.53	0.120E−08
(37)	$CH_3^+ + C_2H_6 \rightarrow C_2H_5^+ + CH_4$	0.85	0.174E−08
(38)	$CH_3^+ + N \rightarrow H_2CN^+ + H$	1.00	0.670E−10
(39)	$CH_4^+ + H_2 \rightarrow CH_5^+ + H$	1.00	0.330E−10
(40)	$CH_4^+ + CH_4 \rightarrow CH_5^+ + CH_3$	1.00	0.150E−08
(41)	$CH_4^+ + C_2H_2 \rightarrow C_2H_2^+ + CH_4$	0.45	0.252E−08
(42)	$CH_4^+ + C_2H_2 \rightarrow C_2H_3^+ + CH_3$	0.49	0.252E−08
(43)	$CH_4^+ + C_2H_4 \rightarrow C_2H_5^+ + CH_3$	0.23	0.184E−08
(44)	$CH_4^+ + H_2O \rightarrow H_3O^+ + CH_3$	1.00	0.250E−08
(45)	$CH_4^+ + HCN \rightarrow H_2CN^+ + CH_3$	0.98	0.330E−08
(46)	$CH_5^+ + H \rightarrow CH_4^+ + H_2$	1.00	0.150E−09
(47)	$CH_5^+ + C_2H_2 \rightarrow C_2H_3^+ + CH_4$	1.00	0.156E−08
(48)	$CH_5^+ + C_2H_4 \rightarrow C_2H_5^+ + CH_4$	1.00	0.150E−08
(49)	$C_2H^+ + H_2 \rightarrow C_2H_2^+ + H$	1.00	0.170E−08
(50)	$C_2H^+ + CH_4 \rightarrow C_2H_2^+ + CH_3$	0.34	0.110E−08
(51)	$C_2H^+ + N \rightarrow CH^+ + CN$	1.00	0.900E−10
(52)	$C_2H^+ + HCN \rightarrow H_2CN^+ + C_2$	0.50	0.270E−08
(53)	$C_2H^+ + HCN \rightarrow HC_3N^+ + H$	0.50	0.270E−08
(54)	$C_2H^+ + HC_3N \rightarrow HC_3N^+ + C_2H$	0.10	0.320E−08
(55)	$C_2H_2^+ + H_2 \rightarrow C_2H_3^+ + H$	1.00	0.100E−10
(56)	$C_2H_2^+ + C_2H_6 \rightarrow C_2H_5^+ + C_2H_3$	0.09	0.146E−08
(57)	$C_2H_2^+ + N \rightarrow CH^+ + HCN$	0.10	0.250E−09
(58)	$C_2H_2^+ + N \rightarrow C_2N^+ + H_2$	0.30	0.250E−09
(59)	$C_2H_2^+ + HCN \rightarrow H_2CN^+ + C_2H$	0.66	0.360E−09
(60)	$C_2H_3^+ + C_2H_2 \rightarrow C_2H_3^+ + C_2H_2$	0.70	0.720E−09
(61)	$C_2H_3^+ + C_2H_4 \rightarrow C_2H_5^+ + C_2H_2$	1.00	0.930E−09
(62)	$C_2H_3^+ + C_2H_6 \rightarrow C_2H_5^+ + C_2H_4$	0.47	0.620E−09
(63)	$C_2H_3^+ + HCN \rightarrow H_2CN^+ + C_2H_2$	1.00	0.290E−08
(64)	$C_2H_3^+ + C_2N_2 \rightarrow HC_2N_2^+ + C_2H_2$	0.80	0.710E−09
(65)	$C_2H_5^+ + HCN \rightarrow H_2CN^+ + C_2H_4$	1.00	0.270E−08
(66)	$C_2H_6^+ + C_2H_2 \rightarrow C_2H_5^+ + C_2H_3$	0.19	0.177E−08
(67)	$C_3H^+ + CH_4 \rightarrow C_2H_3^+ + C_2H_2$	0.70	0.550E−09
(68)	$C_3H^+ + HCN \rightarrow H_2CN^+ + C_3$	0.01	0.110E−08
(69)	$N^+ + HCN \rightarrow CH_3^+ + NH$	0.53	0.135E−08
(70)	$N^+ + HCN \rightarrow CH_4^+ + N$	0.04	0.135E−08
(71)	$N^+ + HCN \rightarrow H_2CN^+ + H_2$	0.32	0.135E−08
(72)	$N^+ + HCN \rightarrow HCN^+ + H_2$	0.10	0.135E−08
(73)	$N^+ + CH_4 \rightarrow CH_3^+ + NH$	0.53	0.135E−08
(74)	$N^+ + CH_4 \rightarrow CH_4^+ + N$	0.04	0.135E−08
(75)	$N^+ + CH_4 \rightarrow H_2CN^+ + H_2$	0.32	0.135E−08
(76)	$N^+ + CH_4 \rightarrow HCN^+ + H_2$	0.10	0.135E−08
(77)	$N^+ + C_2H_4 \rightarrow C_2H_2^+ + NH_2$	0.10	0.160E−08
(78)	$N^+ + C_2H_4 \rightarrow C_2H_3^+ + NH$	0.30	0.160E−08
(79)	$N^+ + C_2H_4 \rightarrow HCN^+ + CH_3$	0.15	0.160E−08
(80)	$N^+ + C_2H_4 \rightarrow H_2CN^+ + CH_2$	0.10	0.160E−08
(81)	$N^+ + C_2N_2 \rightarrow C_2N_2^+ + N$	0.30	0.140E−08
(82)	$N^+ + C_2N_2 \rightarrow C_2N^+ + N_2$	0.70	0.140E−08
(83)	$N^+ + HC_3N \rightarrow C_3H^+ + N_2$	0.50	0.420E−08
(84)	$N^+ + HC_3N \rightarrow HC_3N^+ + N$	0.50	0.420E−08
(85)	$N_2^+ + H_2 \rightarrow N_2H^+ + H$	1.00	0.210E−08
(86)	$N_2^+ + CH_4 \rightarrow CH_3^+ + N_2$	0.92	0.980E−09
(87)	$N_2^+ + CH_4 \rightarrow CH_2^+ + N_2$	0.08	0.980E−09
(88)	$N_2^+ + C_2H_2 \rightarrow C_2H_2^+ + N_2$	1.00	0.430E−09
(89)	$N_2^+ + N \rightarrow N^+ + N_2$	1.00	0.100E−10
(90)	$N_2^+ + Ar \rightarrow Ar^+ + N_2$	1.00	0.200E−12
(91)	$N_2^+ + HCN \rightarrow HCN^+ + N_2$	1.00	0.390E−09
(92)	$N_2^+ + HC_3N \rightarrow HC_3N^+ + N_2$	1.00	0.410E−08
(93)	$N_2^+ + C_2N_2 \rightarrow C_2N_2^+ + N_2$	1.00	0.860E−09
(94)	$N_2^+ + CO \rightarrow CO^+ + N_2$	1.00	0.740E−10
(95)	$N_2^+ + CO_2 \rightarrow CO_2^+ + N_2$	1.00	0.900E−09
(96)	$N_2H^+ + H_2 \rightarrow H_3^+ + N_2$	1.00	0.510E−17
(97)	$N_2H^+ + CH_4 \rightarrow CH_5^+ + N_2$	1.00	0.890E−09
(98)	$N_2H^+ + C_2H_2 \rightarrow C_2H_3^+ + N_2$	1.00	0.141E−08
(99)	$N_2H^+ + C_2H_6 \rightarrow C_2H_5^+ + N_2$	0.87	0.130E−08
(100)	$N_2H^+ + HCN \rightarrow H_2CN^+ + N_2$	1.00	0.320E−08
(101)	$N_2H^+ + C_2N_2 \rightarrow HC_2N_2^+ + N_2$	1.00	0.120E−08
(102)	$Ar^+ + H_2 \rightarrow ArH^+ + H$	1.00	0.880E−09
(103)	$Ar^+ + CH_4 \rightarrow CH_3^+ + Ar$	0.85	0.103E−08
(104)	$Ar^+ + CH_4 \rightarrow CH_2^+ + Ar$	0.15	0.103E−08
(105)	$Ar^+ + N_2 \rightarrow N_2^+ + Ar$	1.00	0.100E−10
(106)	$ArH^+ + H_2 \rightarrow H_3^+ + Ar$	1.00	0.800E−09
(107)	$ArH^+ + CH_4 \rightarrow CH_5^+ + Ar$	1.00	0.110E−08
(108)	$ArH^+ + C_2H_4 \rightarrow C_2H_3^+ + Ar$	0.73	0.115E−08
(109)	$ArH^+ + C_2H_4 \rightarrow C_2H_5^+ + Ar$	0.27	0.115E−08
(110)	$ArH^+ + C_2H_6 \rightarrow C_2H_3^+ + Ar$	0.04	0.140E−08
(111)	$ArH^+ + C_2H_6 \rightarrow C_2H_5^+ + Ar$	0.96	0.140E−08
(112)	$ArH^+ + N_2 \rightarrow N_2H^+ + Ar$	1.00	0.800E−09
(113)	$CN^+ + H_2 \rightarrow HCN^+ + H$	1.00	0.100E−08
(114)	$CN^+ + CH_4 \rightarrow CH_3^+ + HCN$	0.50	0.900E−09

TABLE 2—*Continued*

	Process		Branching Ratio	Rate Coefficient
(115)	$CN^+ + CH_4 \rightarrow CH_4^+ + CN$		0.15	0.900E−09
(116)	$CN^+ + CH_4 \rightarrow HCN^+ + CH_3$		0.15	0.900E−09
(117)	$CN^+ + CH_4 \rightarrow H_2CN^+ + CH_2$		0.10	0.900E−09
(118)	$CN^+ + C_2H_2 \rightarrow C_2H_2^+ + CN$		0.90	0.150E−08
(119)	$CN^+ + C_2H_2 \rightarrow HC_3N^+ + H$		0.10	0.150E−08
(120)	$CN^+ + C_2H_4 \rightarrow HCN^+ + C_2H_3$		0.25	0.100E−08
(121)	$CN^+ + C_2H_6 \rightarrow C_2H_3^+ + HCN$		0.15	0.190E−08
(122)	$CN^+ + C_2H_6 \rightarrow C_2H_5^+ + HCN$		0.20	0.190E−08
(123)	$CN^+ + HCN \rightarrow HCN^+ + CN$		0.85	0.210E−08
(124)	$CN^+ + HCN \rightarrow C_2N_2^+ + H$		0.15	0.210E−08
(125)	$CN^+ + HC_3N \rightarrow HC_3N^+ + CN$		0.80	0.390E−08
(126)	$CN^+ + HC_3N \rightarrow C_3N^+ + HCN$		0.20	0.390E−08
(127)	$CN^+ + C_2N_2 \rightarrow C_2N_2^+ + CN$		0.85	0.140E−08
(128)	$CN^+ + C_2N_2 \rightarrow C_3N^+ + N_2$		0.10	0.140E−08
(129)	$CN^+ + C_2N_2 \rightarrow C_2N^+ + CN_2$		0.05	0.140E−08
(130)	$HCN^+ + H_2 \rightarrow H_2CN^+ + H$		1.00	0.980E−09
(131)	$HCN^+ + CH_4 \rightarrow H_2CN^+ + CH_3$		0.50	0.140E−08
(132)	$HCN^+ + CH_4 \rightarrow C_2H_3^+ + NH_2$		0.50	0.140E−08
(133)	$HCN^+ + C_2H_2 \rightarrow C_2H_2^+ + HCN$		0.60	0.690E−09
(134)	$HCN^+ + C_2H_2 \rightarrow H_2CN^+ + C_2H$		0.10	0.690E−09
(135)	$HCN^+ + C_2H_2 \rightarrow C_2H_3^+ + CN$		0.10	0.690E−09
(136)	$HCN^+ + HCN \rightarrow H_2CN^+ + CN$		1.00	0.160E−08
(137)	$HCN^+ + HC_3N \rightarrow HC_3N^+ + HCN$		0.52	0.460E−08
(138)	$C_2N^+ + CH_4 \rightarrow C_2H_3^+ + HCN$		1.00	0.440E−11
(139)	$C_2N^+ + C_2H_2 \rightarrow C_3H^+ + HCN$		0.80	0.100E−08
(140)	$C_2N^+ + C_2H_6 \rightarrow C_2H_3^+ + CH_3CN$		0.10	0.120E−08
(141)	$C_2N^+ + C_2H_6 \rightarrow C_2H_5^+ + HC_2N$		0.25	0.120E−08
(142)	$C_2N^+ + HC_3N \rightarrow C_3H^+ + C_2N_2$		1.00	0.310E−08
(143)	$C_3N^+ + H_2 \rightarrow HC_3N^+ + H$		0.90	0.910E−09
(144)	$HC_3N^+ + H_2 \rightarrow C_2H_2^+ + HCN$		0.24	0.700E−11
(145)	$C_2N_2^+ + HC_3N \rightarrow HC_3N^+ + C_2N_2$		1.00	0.160E−08
(146)	$HC_2N_2^+ + C_2H_4 \rightarrow C_2H_5^+ + C_2N_2$		0.70	0.560E−09

adopted two models: the first one (model L) assumes that the mixing ratio of CH_4 remains constant at 0.1 for altitude (z) > 1200 km; in the second one (model H) the mixing ratio of CH_4 increases to 0.6 at z = 2200 km and then stays constant. The vertical profiles of the neutral species are then used as inputs for the ionospheric model calculations. A more reliable approach would require a comprehensive coverage of the neutral gas distributions to altitudes much larger than 1200 km. This important information is not yet available at the present moment.

b) Velocity Profiles

i) *One-dimensional Subsonic Inflow*

Detailed investigations of the global plasma interaction of the magnetospheric flow with Titan's atmosphere require numerical magnetohydrodynamic (MHD) simulations. If we are primarily interested in the dynamical effects on the structure of the upper ionosphere, some simplified treatments can still be used to illustrate a few of the salient features. For example, to answer the question how far the plasma flow would be able to penetrate the neutral atmosphere, we can first use a one-dimensional, steady state, one-fluid model to describe the inward streaming of the plasma flow. The basic equations for a mass-loaded flow are (Wallis 1973; Galeev, Cravens, and Gombosi 1985)

TABLE 3

LIST OF ELECTRON IMPACT IONIZATION PROCESSES

(1)	H_2	$+ e \rightarrow H_2^+ + 2e$	
(2)	CH_4	$+ e \rightarrow CH_3^+ + H + 2e$	
(3)	CH_4	$+ e \rightarrow CH_4^+ + 2e$	
(4)	C_2H_2	$+ e \rightarrow C_2H^+ + H + 2e$	
(5)	C_2H_2	$+ e \rightarrow C_2H_2^+ + 2e$	
(6)	C_2H_4	$+ e \rightarrow C_2H_3^+ + H + 2e$	
(7)	C_2H_6	$+ e \rightarrow C_2H_5^+ + H + 2e$	
(8)	C_2H_6	$+ e \rightarrow C_2H_6^+ + 2e$	
(9)	N	$+ e \rightarrow N^+ + 2e$	
(10)	N_2	$+ e \rightarrow N_2^+ + 2e$	
(11)	N_2	$+ e \rightarrow N^+ + N + 2e$	
(12)	HCN	$+ e \rightarrow CN^+ + H + 2e$	
(13)	HCN	$+ e \rightarrow HCN^+ + 2e$	
(14)	C_2N_2	$+ e \rightarrow C_2N^+ + N + 2e$	
(15)	HC_3N	$+ e \rightarrow HC_3N^+ + 2e$	

TABLE 4

LIST OF ELECTRON DISSOCIATIVE RECOMBINATION COEFFICIENTS[a]

	Ion			α
(1)	H_2^+	$+ e \rightarrow H$	$+ H$	1.0 E−7
(2)	H_3^+	$+ e \rightarrow H_2$	$+ H$	4.1 E−7[b]
(3)	CH^+	$+ e \rightarrow C$	$+ H$	1.0 E−7
(4)	CH_2^+	$+ e \rightarrow CH$	$+ H$	5.1 E−7
(5)	CH_3^+	$+ e \rightarrow CH_2$	$+ H$	7.6 E−7[b]
(6)	CH_4^+	$+ e \rightarrow CH_3$	$+ H$	6.0 E−7[b]
(7)	CH_5^+	$+ e \rightarrow CH_4$	$+ H$	7.0 E−7
(8)	C_2H^+	$+ e \rightarrow C_2$	$+ H$	1.9 E−6
(9)	$C_2H_2^+$	$+ e \rightarrow C_2H$	$+ H$	6.0 E−7[b]
(10)	$C_2H_3^+$	$+ e \rightarrow C_2H_2$	$+ H$	9.5 E−7
(11)	$C_2H_5^+$	$+ e \rightarrow C_2H_2$	$+ H_2 + H$	1.9 E−6
(12)	$C_2H_6^+$	$+ e \rightarrow C_2H_4$	$+ H_2$	1.9 E−6
(13)	C_3H^+	$+ e \rightarrow C_3$	$+ H$	1.9 E−6
(14)	N^+	$+ e \rightarrow N$		1.0 E−12
(15)	N_2^+	$+ e \rightarrow N$	$+ N$	3.6 E−7
(16)	N_2H^+	$+ e \rightarrow N_2$	$+ H$	7.6 E−7
(17)	H_2O^+	$+ e \rightarrow O$	$+ H_2$	7.6 E−7
(18)	H_3O^+	$+ e \rightarrow H_2O$	$+ H$	7.0 E−7[b]
(19)	Ar^+	$+ e \rightarrow Ar$		1.0 E−12
(20)	ArH^+	$+ e \rightarrow Ar$	$+ H$	1.0 E−7
(21)	CN^+	$+ e \rightarrow C$	$+ N$	5.0 E−7
(22)	HCN^+	$+ e \rightarrow H$	$+ CN$	5.0 E−7
(23)	H_2CN^+	$+ e \rightarrow HCN$	$+ H$	6.3 E−7
(24)	C_2N^+	$+ e \rightarrow CN$	$+ N$	3.0 E−7[c]
(25)	C_3N^+	$+ e \rightarrow C_2$	$+ CN$	3.0 E−7[c]
(26)	HC_3N^+	$+ e \rightarrow HCN$	$+ C_2$	3.0 E−7[c]
(27)	$C_2N_2^+$	$+ e \rightarrow C_2$	$+ N_2$	3.0 E−7[c]
(28)	$HC_2N_2^+$	$+ e \rightarrow HCN$	$+ CN$	3.0 E−7[c]
(29)	CO^+	$+ e \rightarrow C$	$+ O$	5.0 E−7
(30)	HCO^+	$+ e \rightarrow H$	$+ CO$	2.0 E−7
(31)	CO_2^+	$+ e \rightarrow CO$	$+ O$	3.8 E−7
(32)	HCO_2^+	$+ e \rightarrow CO_2$	$+ H$	6.4 E−7[b]

[a] From Schmidt *et al.* 1988.
[b] Sum of multiple channels.
[c] Guestimated value.

Mass continuity:

$$\frac{1}{A}\frac{d}{ds}(A\rho w) = (q - l)m_i\,, \tag{6}$$

Momentum:

$$\frac{1}{A}\frac{d}{ds}(A\rho w) = -\frac{dp}{ds} - \frac{1}{8\pi}\frac{dB^2}{ds} + \frac{B^2}{4\pi r_c} - \rho w \nu_{in}\,, \tag{7}$$

Energy:

$$\frac{1}{A}\frac{d}{ds}\left[Aw\left(\frac{\rho w^2}{2} + \frac{\gamma}{\gamma - 1}p + \frac{B^2}{4\pi}\right)\right] = 0\,. \tag{8}$$

In the above equations, ρ is the mass density of the plasma, w the flow velocity, p the thermal pressure, B the magnetic field, A the cross section of the stream tube, q the ionization rate of the neutral atmosphere, l the loss rate due to electron dissociative recombination, γ the ratio of the specific heats, m_i the mass of the exospheric ions, ν_{in} the ion-neutral collision frequency, and, finally, r_c the radius of curvature of the magnetic field lines draped by Titan's ionosphere. The application of these equations implies that Titan's plasma interaction, to a certain degree, should be similar to that of comet–solar wind interaction characterized by the mass-loading effect and ion-neutral friction in the atmosphere (Ip and Axford 1990). Assuming the corotating plasma flow to be subsonic, we have further included the following incompressibility relation:

$$Aw = 0\,, \tag{9}$$

such that the pressure gradient dp/ds is nearly zero in this region. Figure 3 depicts the flow profiles for three starting values of streaming velocity: (*a*) $w_0 = 110$ km s^{-1}, (*b*) $w_0 = 10$ km s^{-1}, and (*c*) $w_0 = 1$ km s^{-1}. In these calculations, the initial Mach number is $M = 0.35$ and the magnetic field $B = 0$. The ion-neutral frictional force, as given in the last term on the right-hand side of equation (7), plays a crucial role in stopping the ionospheric inflow at a certain distance above the exobase at $z = 1400$ km. For fast inflow ($w_0 = 100$ km s^{-1}), the stopping distance is at $z \approx 1600$ km, while an extremely slow flow ($w_0 = 10$ km s^{-1}) would stop at $z \approx 2300$ km. The exact global velocity profile and magnetic field variation (which is omitted here) would have to be computed by using a more comprehensive electrodynamic model.

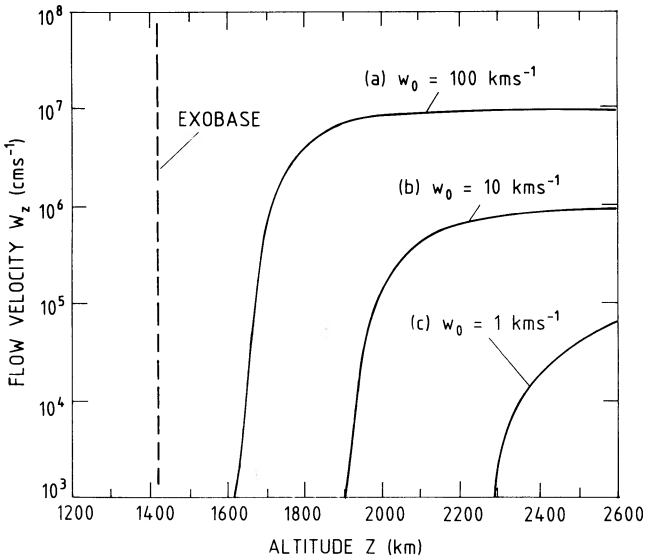

FIG. 3.—Flow profiles of the corotating magnetospheric plasma obtained from a one-fluid mass-loading approximation: (*a*) the initial vertical streaming velocity $w_0 = 100$ km s^{-1}, (*b*) $w_0 = 10$ km s^{-1}, and (*c*) $w_0 = 1$ km s^{-1}.

ii) *One-dimensional Convection-Diffusion Approximation*

Note that as the ionospheric flow enters the dense region of the atmosphere, the plasma motion can be more accurately described in the convection-diffusion approximation. In this limit, the full set of equations of ionospheric motion can be written as (Banks and Kockarts 1973)

$$x:\quad v_i\Omega_z^i = \nu_{in}(u_i - u_n) - \left(\frac{eE_x}{m_i}\right), \tag{10}$$

$$v_e\Omega_z^e = -\nu_{en}(u_e - u_n) - \left(\frac{eE_x}{m_e}\right), \tag{11}$$

$$y:\quad u_i\Omega_z^i = w_i\Omega_x^i - \nu_n(v_i - v_n) + \left(\frac{eE_y}{m_i}\right), \tag{12}$$

$$u_e\Omega_z^e = w_e\Omega_x^e + \nu_{en}(v_e - v_n) + \left(\frac{eE_y}{m_e}\right), \tag{13}$$

$$z:\quad \frac{1}{n_i m_i}\frac{\partial p_i}{\partial z} + g - \frac{eE_z}{m_i} + \nu_i\Omega_x^i = -\nu_{in}(w_i - w_n)\,, \tag{14}$$

$$\frac{1}{n_e m_e}\frac{\partial p_e}{\partial z} + g + \frac{eE_z}{m_e} - \nu_e\Omega_x^e = -\nu_{en}(w_e - w_n)\,. \tag{15}$$

In the above equations, the plasma flow velocities are designated as $\boldsymbol{u}_i = (u_i, v_i, w_i)$ for the ions and $\boldsymbol{u}_e = (u_e, v_e, w_e)$ for the electrons. The neutral gas molecules are assumed to be stationary; thus $\boldsymbol{u}_n = 0$. The collisional frequency of ions with the neutral gas is given as

$$\nu_{in} = 3.9 \times 10^{-10} n \quad \text{s}^{-1}, \tag{16}$$

and the electron-neutral collision frequency is

$$\nu_{en} = 1.6 \times 10^{-9} T_e^{1/2} n \quad \text{s}^{-1}\,, \tag{17}$$

where n is the number density of the neutral gas.

Assuming that the magnetic field is horizontal and points to the x-axis, i.e., $\boldsymbol{B} = (B_0\,\phi, 0, 0)$, with B_0 as the initial value at large vertical distance from the exobase and $\phi(z)$ a function of the altitude z, and that the electric field $\boldsymbol{E}$ can be expressed as $\boldsymbol{E} = (0, E_y, E_z)$, with $E_y = -W_0 B_0/c$, where W_0 is the initial plasma speed in the vertical direction, the equations of motion in the y- and z-directions for one single ion species can be simplified as

$$y:\quad w_i\Omega_i - \nu_{in} v_i + \frac{eE_y}{m_i} = 0\,, \tag{18}$$

$$w_e\Omega_e + \nu_{en} v_e + \frac{eE_y}{m_e} = 0\,, \tag{19}$$

$$z:\quad v_i\Omega_i + \nu_{in} w_i - \frac{eE_z}{m_i} = 0\,, \tag{20}$$

$$-v_e\Omega_e + \nu_{en} w_e + \frac{eE_z}{m_e} = 0\,, \tag{21}$$

with $\Omega_i = eB_0\,\phi/m_i c$ and $\Omega_e = eB_0\,\phi/m_e c$.

Note that the pressure gradient terms and the gravity term

are neglected in the above equations. From the elimination of the E_z term in equations (20) and (21), we obtain

$$m_i v_i \Omega_i + m_e v_e \Omega_e + m_i \nu_{in} w_i + m_e \nu_{en} w_e = 0 . \quad (22)$$

The substitution of v_i and v_e terms from equations (18) and (19) into the above equation yields

$$m_i \nu_{in} w_i \left[1 + \left(\frac{\Omega_i}{\nu_{in}}\right)^2 \phi^2\right] + m_e \nu_{en} w_e \left[1 + \left(\frac{\Omega_e}{\nu_{en}}\right)^2 \phi^2\right] + eE_0 \left(\frac{\Omega_i}{\nu_{in}} + \frac{\Omega_e}{\nu_{en}}\right)\phi = 0 . \quad (23)$$

From $w_i = w_e$ we obtain the final expression of the plasma flow speed under the influence of convection and diffusion:

$$w_i = \frac{eE_0(\Omega_i/\nu_{in} + \Omega_e/\nu_{in})\phi}{m_i \nu_{in}[1 + (\Omega_i/\nu_{in})^2\phi^2] + m_e \nu_{en}[1 + (\Omega_e/\nu_{en})^2\phi^2]} . \quad (24)$$

From the Maxwell equation,

$$\nabla \times B = \frac{4\pi}{c} j , \quad (25)$$

where the horizontal electric current j is written as

$$j = (n_i v_i - n_e v_e)e \quad (26)$$

$$= \left(\frac{\Omega_i}{\nu_{in}} + \frac{\Omega_e}{\nu_{en}}\right)\left(w_i \phi + \frac{eE_y}{B}\right)e , \quad (27)$$

we have

$$B_0 \frac{d\phi}{dz} = \frac{4\pi e}{c}\left(\frac{\Omega_i}{\nu_{in}} + \frac{\Omega_e}{\nu_{en}}\right)\left(w_i \phi + \frac{cE_y}{B}\right) . \quad (28)$$

The combination of equations (4), (24), and (28) provides a self-consistent description of the ionospheric density and plasma flow profile in the context of a one-dimensional model. This one-dimensional model was first applied to the Martian ionosphere by Axford and Johnson (1972) in an unpublished work. Their results were shown to be remarkably similar to a more comprehensive MHD simulation by Shinagawa and Cravens (1989). The coupled equations as discussed here thus might serve as a first approximation to the structure of Titan's upper ionosphere, even though the pressure gradient effect is omitted in the treatment.

Figure 4 illustrates an example of the variations of the horizontal magnetic field and the inflow velocity as a function of altitude in the ionospheric environment of Titan. The starting value of the magnetic field is $B_0 = 10nT$ and the initial downward flow speed is -8 m s^{-1}. The increasing neutral friction effect near the exobase leads to a sharp drop of the magnetic field as well as the flow speed at $z \approx 1200$ km. The characteristic half-width of the velocity and magnetic field changes is about 60 km.

Thus in the present one-dimensional convection-diffusion approximation, a magnetic field–free region in the lower ionosphere of Titan is predicted. The possible occurrence of ionospheric instabilities, as discussed before for the magnetic flux ropes of Venus (Wolff, Goldstein, and Yeates 1980; Elphic and Ershkovich 1984), might permit the infiltration of magnetic field irregularities into this field–free region, however.

At high-altitude regions, lateral flow in the horizontal direction could take place to drain away the ions. Shinagawa and Cravens (1989), for example, have found that in the case of

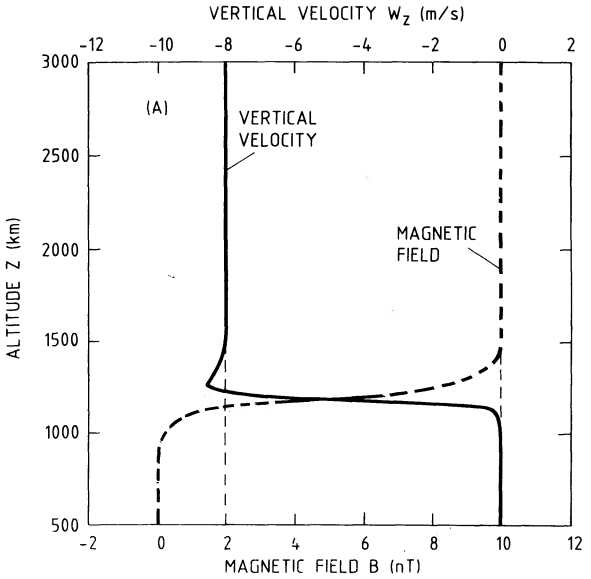

FIG. 4.—Vertical velocity and magnetic field variations obtained from a one-dimensional diffusion-convection approximation.

Mars a rather significant horizontal convection effect must be included to account for the observed ionospheric profile above 300 km altitude. To approximate this effect, we have computed the ionospheric profiles at different starting positions where the total ion density $n_i = 0$: (*a*) $z_0 = \infty$, (*b*) $z_0 = 3000$ km, and (*c*) $z_0 = 2500$ km; see Figure 5. It can be seen that, in the steady state situation, as soon as the horizontal convection ceases to be significant, the ionospheric profile will quickly recover the structure predicted in a one-dimensional chemical equilibrium model.

III. ION COMPOSITION

In order to examine the coupled effect of the chemical network on the ionospheric composition of Titan, the iono-

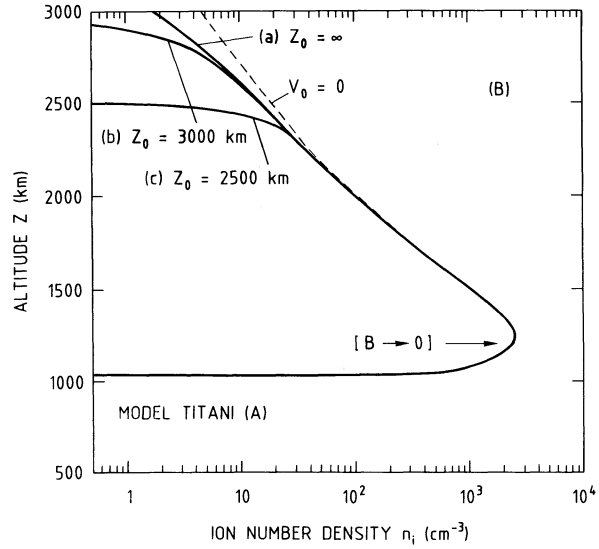

FIG. 5.—Total ion density (n_i) profile derived from assuming $n_i = 0$ at (*a*) $z_0 = \infty$, (*b*) $z_0 = 3000$ km, and (*c*) $z_0 = 2500$ km. Note that the sharp drop of the n_i value at $z \approx 1000$ km is due to the omission of cosmic-ray ionization in the calculations.

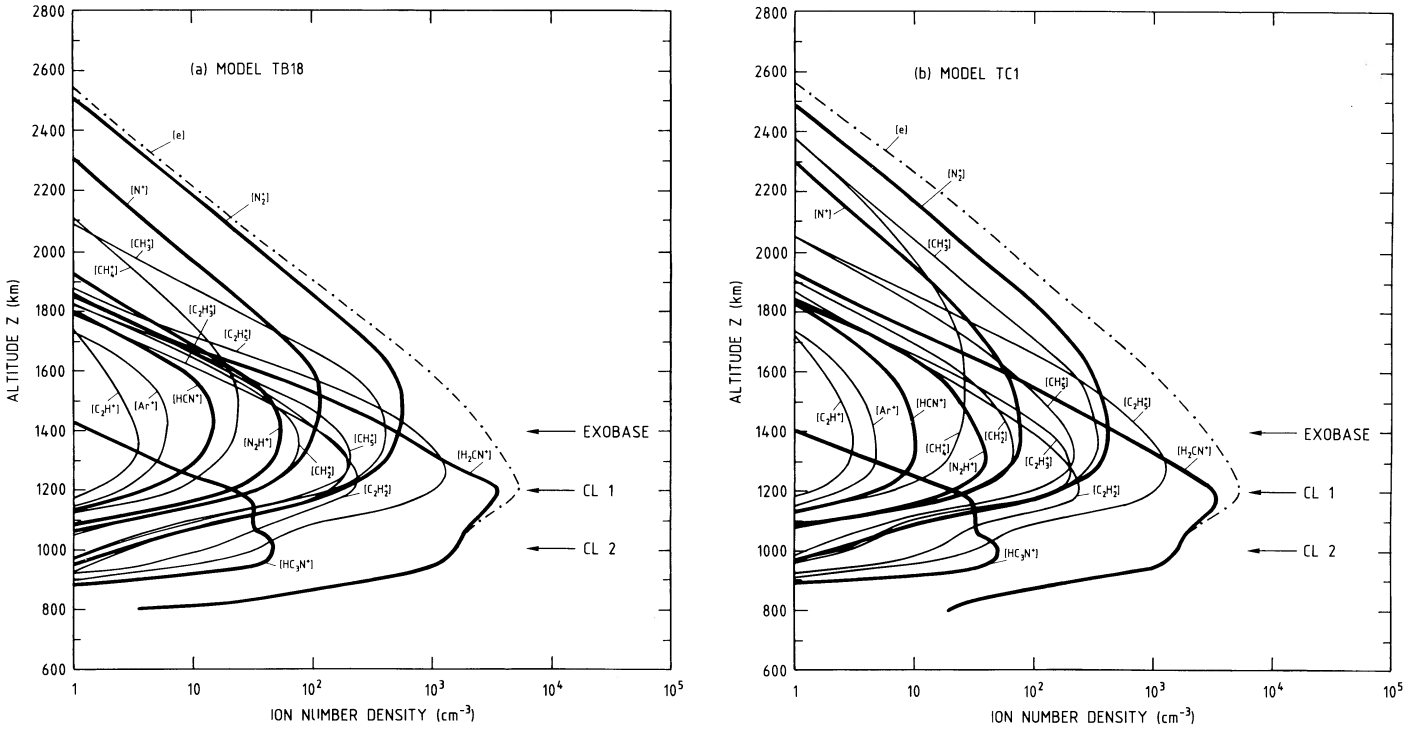

FIG. 6.—Vertical distributions of the number densities of several major ion species from chemical equilibrium model calculations: (*a*) low CH_4 mode and (*b*) high CH_4 model.

spheric profiles for several different velocity models are computed. The case of stationary chemical equilibrium with low (high) CH_4 mixing ratio is illustrated in Figure 6*a* (6*b*). As mentioned before, the electron density peak from electron impact ionization is located at about 1240 km altitude (e.g., CL1 in Fig. 6; see Bauer 1985; McNutt and Richardson 1988). Above this peak, the N_2^+ ion is the dominant ion species. This is followed by the CH_3^+ ion, which is produced from direct electron impact ionization and ion-molecule reaction involving N_2^+ and CH_4. As shown in the chemical scheme in Figure 7*a*, the CH_3^+ ion is lost via ion-molecule reactions with the CH_4, C_2H_4, and C_2H_6 molecules as well as electron dissociative recombination. Without these loss mechanisms, CH_3^+ ions will accumulate to be the most abundant ions in the upper ionosphere. This effect in fact explains the basic difference in our chemical model and that of Bauer (1985), which has a CH_3^+–dominated ionosphere.

A large quantity of N^+ ions are created via electron impact of the nitrogen gas. These atomic ions are lost rapidly as a result of the ion-neutral reaction with CH_4.

The $C_2H_5^+$ ion, which is created via the ion-molecule reaction between CH_3^+ and CH_4 and is lost only through electron dissociative recombination in the present chemical network (see Fig. 7*b*), becomes the fourth most abundant ion species (after N_2^+, N^+, and CH_3^+) for $z > 1400$ km. At z between 1200 and 1400 km, the $C_2H_5^+$ ion is the most dominant ion. The H_2CN^+ ion, which is created via ion-molecule reaction between HCN^+ and CH_4 and other channels (see Fig. 7*c*), will take over at lower altitudes and becomes the most important ion species for $z < 1200$ km.

The inclusion of the photoionization effect leads to the formation of another electron density peak (e.g., CL2) at ≈ 1000 km altitude. As discussed in § II*b*(i), the large-scale magnetic field could only penetrate to an altitude of about 1200 km. No magnetospheric electrons with $E \leq 1$ keV would be able to reach the lower region. The photoionization effect should then play a crucial role as the main ionization mechanism for altitudes between 900 and 1200 km. The occurrence of instabilities at the magnetic field–free boundary might lead to the further infiltration of magnetic field in the form of magnetic flux ropes as observed at Venus. An overlapping of the electron impact ionization and photoionization below 1200 km altitude is therefore possible. Beginning at $z \lesssim 700$ km, the GCR induced ionization will be the main source mechanism for the lower ionosphere where synthesis of complex organic molecules could occur (Capone *et al.* 1980, 1981).

Besides the five major ions (N_2^+, N^+, CH_3^+, $C_2H_5^+$, and H_2CN^+) with peak densities reaching values larger than 100 cm^{-3}, there are many others with significant abundances in such a stationary chemical-equilibrium ionosphere; examples are the CH_2^+, CH_4^+, $C_2H_3^+$, and N_2H^+ ions. They all reach corresponding peak densities at z between 1200 and 1400 km. However, such predicted compositional distributions are not necessarily applicable at higher altitude. First, the uncertainty in the relative abundance of CH_4 could lead to very different ion composition therein. Second, the convection effect of the streaming plasma could compress the ionospheric profile downward until it is stopped by the thermal pressure of Titan's ionosphere or by the neutral friction of the dense atmosphere.

In addition to the suite of molecular ions as illustrated in Figure 6, we have investigated the production of Ar^+ ions (with the assumption that the argon mixing ratio is about 10^{-2} at the homopause) and found that their peak number density should be $\lesssim 10$ cm^{-3} as a result of fast reactions with CH_4 and N_2. (For larger abundance of Ar, the Ar^+ number density will be proportionally enhanced.) On the other hand, metallic ions such as Na^+ and Fe^+ which do not react strongly with the major neutral species in Titan's atmosphere would be prefer-

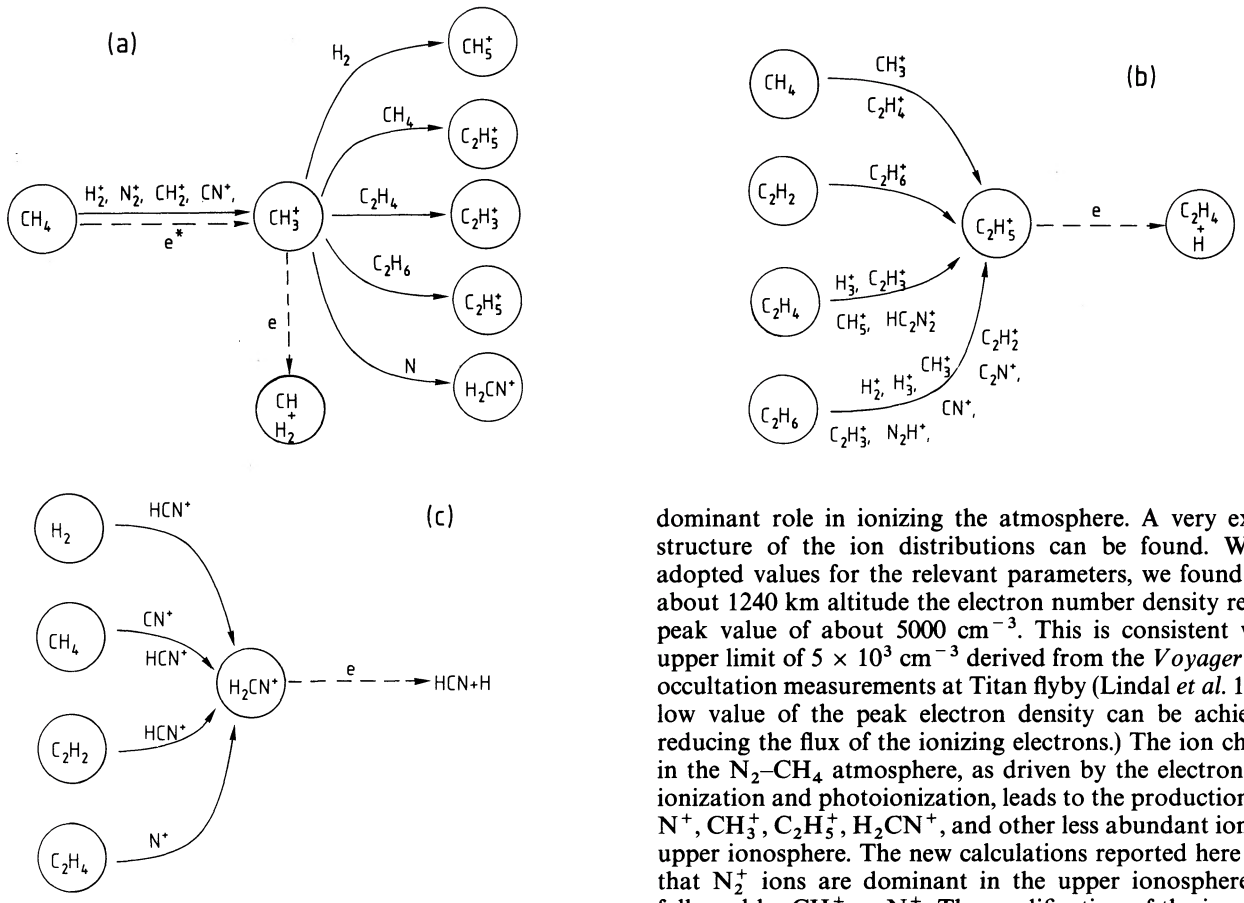

FIG. 7.—Major chemical networks leading to the production and destruction of (*a*) the CH_3^+ ions, (*b*) the $C_2H_5^+$ ions, and (*c*) the H_2CN^+ ions.

entially accumulated in the ionosphere as a result of their very slow electron radiative recombination loss process. It is also possible that thin layers of Na^+ and Fe^+ ions from meteoroid ablation could form under the action of neutral wind. (See Nygren *et al.* 1984 for a recent discussion on the formation of sporadic *E*-layers in the terrestrial ionosphere.)

The ionospheric profiles displayed in Figures 6*a* and 6*b* are basically deduced from model (*a*) (§ II*b*[ii]) with $z_0 = \infty$ in Figure 5, i.e., no vertical compression or lateral flow. In order to examine the effect of a lateral flow, we have also computed the ion density distributions for case (*b*) with $z_0 = 3000$ km and case (*c*) with $z_0 = 2500$ km (at which point $n_i = 0$). The general pattern is for the formation of an ionopause-like structure at z_0 below which the ion composition quickly recovers to the distributions shown in Figure 6.

In the above calculations, the numerical stability of the multispecies system is achieved by setting the vertical flow speed to be constant at $w_z = 10$ m s^{-1}. At such low flow speed, the condition of chemical equilibrium is largely satisfied. A more comprehensive model would require computation of the flow profiles of different species as well as the ion and electron temperatures.

IV. SUMMARY AND DISCUSSION

We have investigated the dynamical effect of magnetospheric plasma flow on the ionospheric profile of Titan. Following the previous work by Bauer (1985) and others, we have considered the case in which magnetospheric electrons play the dominant role in ionizing the atmosphere. A very extensive structure of the ion distributions can be found. With the adopted values for the relevant parameters, we found that at about 1240 km altitude the electron number density reaches a peak value of about 5000 cm^{-3}. This is consistent with an upper limit of 5×10^3 cm^{-3} derived from the *Voyager 1* radio occultation measurements at Titan flyby (Lindal *et al.* 1983). (A low value of the peak electron density can be achieved by reducing the flux of the ionizing electrons.) The ion chemistry in the N_2–CH_4 atmosphere, as driven by the electron impact ionization and photoionization, leads to the production of N_2^+, N^+, CH_3^+, $C_2H_5^+$, H_2CN^+, and other less abundant ions in the upper ionosphere. The new calculations reported here suggest that N_2^+ ions are dominant in the upper ionosphere, to be followed by CH_3^+ or N^+. The modification of the ionospheric structure as a result of plasma interaction was also briefly considered. It has been shown that the direct inflow of the subsonic magnetospheric plasma flow will significantly reduce the ionospheric content flow at high altitudes at $z \geq 2000$ km.

As Titan moves around Saturn, it will encounter different plasma environments in the outer magnetosphere of the planet. For example, the ionizing flux of the suprathermal electrons could change a great deal, and the magnetic field strength could also vary as a function of local time. The exact nature of the ionospheric structure and the magnetosphere-ionosphere interaction hence could be quite complex. The basic effect that the high-altitude ionosphere should be depleted as a result of magnetospheric convection should be present at all times, however. Also, because of the plasma sweeping effect, the Saturnian magnetosphere should be "peppered" with molecular ions such as N_2^+, CH_3^+, $C_2H_5^+$, and H_2CN^+. The plasma plumes emitted from Titan (Eviatar *et al.* 1982), for example, could be enriched in atmospheric ions of such composition.

In the context of one-dimensional treatment, a self-consistent treatment should be given to the ionospheric plasma flows (vertical and horizontal), the magnetic field, and the ion density distribution. This has been done for Venus and Mars (see Shinagawa and Cravens 1988, 1989). We shall attempt similar modeling for Titan in our next step. Another important task to be taken up is to combine the global mass-loading effect with the diffusion-convection process in one single coherent model.

As a final note, it should be mentioned that ultraviolet measurements during the Neptune flyby of the *Voyager 2* spacecraft detected the Neptunian satellite Triton to have a thin atmosphere of nitrogen composition with CH_4 as a minor

component (Broadfoot *et al.* 1989). It is possible that the ionospheric composition and plasma interaction at Triton are similar to those of Titan.

We thank Professor W. I. Axford for bringing our attention to the convection-diffusion approximation of the ionospheric flow, and Professor S. J. Bauer for useful discussions and also J. Cooper for a careful reading of the manuscript. Comments from two anonymous referees were very helpful in improving the manuscript.

REFERENCES

Anicich, V. G., and Huntress, W. T., Jr. 1986, Jet Propulsion Laboratory Preprint, 1986 January 2.
Axford, W. I., and Johnson, H. 1972, paper presented at COSPAR meeting (Madrid).
Banks, P. M., and Kockarts, G. 1973, *Aeronomy, Part B* (New York: Academic), chap. 19.
Bauer, S. J. 1973, *Physics of Planetary Ionospheres* (Berlin–Heidelberg–New York: Springer-Verlag).
———. 1985, in *Proc. Internat. Workshop on Atmospheres of Saturn and Titan* (ESA SP-241), p. 125.
Behannon, K. W., Lepping, R. P., and Ness, N. F. 1983, *J. Geophys. Res.*, **88**, 8791.
Bridge, H. S., *et al.* 1981, *Science*, **212**, 217.
Broadfoot, A. L., *et al.* 1981, *Science*, **212**, 206.
Broadfoot, A. L., *et al.* 1989, *Science*, **246**, 1459.
Capone, L. A., Dubach, J., Whitten, R. C., Prasad, S. S., and Santhanam, K. 1980, *Icarus*, **44**, 72.
Capone, L. A., Prasad, S. S., Huntress, W. T., Whitten, R. C., Dubach, J., and Santhanam, K. 1981, *Nature*, **293**, 45.
Elphic, R. C., and Ershkovich, A. I. 1984, *J. Geophys. Res.*, **89**, 997.
Eviatar, A., Siscoe, G. L., Scudder, J. D., Sittler, E. C., Jr., and Sullivan, J. D. 1982, *J. Geophys. Res.*, **87**, 8091.
Galeev, A. A., Cravens, T. E., and Gombosi, T. I. 1985, *Ap. J.*, **289**, 807.
Hanel, R. A., *et al.* 1981, *Science*, **212**, 192.
Hartle, R. E. 1984, *Adv. Space Res.*, **5** (No. 4), 321.
Hartle, R. E., Sittler, E. C., Jr., Ogilvie, K. W., Scudder, J. D., Lazarus, A. J., and Atreya, S. K. 1982, *J. Geophys. Res.*, **87**, 1383.
Hunten, D. M., Tomasko, M. G., Flasar, F. M., Samuelson, R. E., Strobel, D. F., and Stevenson, D. J. 1984, in *Saturn*, ed. T. Gehrels and M. S. Matthews (Tucson: University of Arizona Press), p. 671.
Ip, W.-H. 1990, *Nature*, **345**, 511.
Ip, W.-H., and Axford, W. I. 1990, in *Physics and Chemistry of Comets*, ed. W. F. Huebner (Heidelberg: Springer-Verlag), in press.
Lindal, G. F., Wood, G. E., Hotz, H. B., and Sweetnam, D. N. 1983, *Icarus*, **53**, 348.
Lutz, B. L., de Bergh, C., and Owen, T. 1983, *Science*, **220**, 1374.
Marten, A., Gautier, D., Tanguy, L., Lecacheux, A., Rosolen, C., and Paubert, G. 1988, *Icarus*, **76**, 558.
McNutt, R. L., Jr., and Richardson, J. D. 1988, *Geophys. Res. Letters*, **15**, 709.
Muhleman, D. O., Berge, G. L., and Clancy, R. T. 1984, *Science*, **220**, 1374.
Naubauer, F. M., Gurnett, D. A., Scudder, J. D., and Hartle, R. E. 1984, in *Saturn*, ed. T. Gehrels and M. S. Matthews (Tucson: University of Arizona Press), p. 760.
Nygren, T., Jalonen, L., Oksman, J., and Turunen, T. 1984, *J. Atm. Terr. Phys.*, **40**, 373.
Owen, T. C. 1982, *Planet. Space Sci.*, **30**, 833.
Russell, C. T., and Vaisberg, O. 1983, in *Venus*, ed. D. M. Hunten, L. Colin, T. M. Donahue, and V. I. Moroz (Tucson: University of Arizona Press), p. 873.
Samuelson, R. E., Hanel, R. A., Kunde, V. G., and Maguire, W. C. 1981, *Nature*, **292**, 688.
Samuelson, R. E., Maguire, W. C., Hanel, R. A., Kunde, V. G., Jennings, D. E., Yung, Y. L., and Aikin, A. C. 1983, *J. Geophys. Res.*, **88**, 8709.
Schmidt, H. U., Wegmann, R., Huebner, W. F., and Boice, D. C. 1988, in *Numerical Simulation of Space Plasmas*, ed. B. Lembege and J. E. Eastwood (Amsterdam: North-Holland), p. 17.
Shinagawa, H., and Cravens, T. E. 1988, *J. Geophys. Res.*, **93**, 11263.
———. 1989, *J. Geophys. Res.*, **94**, 6506.
Sittler, E. C., Jr., Ogilvie, K. W., and Scudder, J. D. 1983, *J. Geophys. Res.*, **88**, 8847.
Smith, G. R., Strobel, D. F., Broadfoot, A. L., Sandel, B. R., Shemansky, D. E., and Holberg, J. B. 1982, *J. Geophys. Res.*, **87**, 1351.
Strobel, D. F. 1974, *Icarus*, **21**, 466.
———. 1982, *Planet. Space Sci.*, **30**, 839.
Strobel, D. F., and Shemansky, D. E. 1982, *J. Geophys. Res.*, **87**, 1361.
Tyler, G. L., Eshleman, V. R., Anderson, J. D., Levy, G. S., Lindal, G. E., Wood, G. E., and Croft, T. A. 1981, *Science*, **212**, 201.
Wallis, M. K. 1973, *Planet. Space Sci.*, **21**, 1647.
Wolff, R. S., Goldstein, B. E., and Yeates, C. M. 1980, *J. Geophys. Res.*, **85**, 7697.
Yung, Y. L., Allen, M., and Pinto, J. P. 1984, *Ap. J. Suppl.*, **55**, 465.

W.-H. Ip: Max-Planck-Institut für Aeronomie, Postfach 20, D-3411 Katlenburg-Lindau, Federal Republic of Germany